Physiological
Measurement

Heart rate variability (HRV) during acute stress: a comparison of three methods for time–frequency analysis

IOP Publishing Physiol. Meas. 47 (2026) 035001 https://doi.org/10.1088/1361-6579/ae3ec7

Physiological Measurement

IPEM Institute of Physics and Engineering in Medicine

PAPER

Heart rate variability (HRV) during acute stress: a comparison of three methods for time–frequency analysis

Bérangère Villatte[1,2,6], **Sayeed A D Kizuk**[1,6], **Jean-Marc Lina**[3,4], **Alain Vinet**[4,5,7] and **Sylvie Hébert**[1,2,7,*]

[1] School of Speech Pathology and Audiology, Faculty of Medicine, Université de Montréal, Québec, Canada
[2] Centre for Interdisciplinary Research on Brain and Learning (CIRCA), Montréal, Québec, Canada
[3] Department of Electrical Engineering, École de Technologie Supérieure (ÉTS), Montréal, Québec, Canada
[4] Centre de Recherche de l'Hôpital du Sacré-Cœur de Montréal, Montréal, Québec, Canada
[5] Department of Pharmacology and Physiology, Faculty of Medicine, Université de Montréal, Québec, Canada
[6] These authors contributed equally to this work and share first authorship.
[7] Senior authors.
[*] Author to whom any correspondence should be addressed.

E-mail: sylvie.hebert@umontreal.ca, Bérangère.villatte@umontreal.ca, sayeed.devraj-kizuk@umontreal.ca, jean-marc.lina@etsmtl.ca and alain.vinet@umontreal.ca

Keywords: time–frequency analysis, short time Fourier transform, empirical mode decomposition, wavelet transform, stress reactivity, heart rate variability, autonomic nervous system

Supplementary material for this article is available online

OPEN ACCESS

RECEIVED
13 August 2025

REVISED
14 January 2026

ACCEPTED FOR PUBLICATION
28 January 2026

PUBLISHED
2 March 2026

Abstract

Objective. Time–frequency (TF) analysis is used to identify oscillatory patterns in complex signals. Cardiac signals under stress conditions are highly dynamic, yet heart rate variability (HRV) is often analysed using classical methods that assume stationarity or linearity. This study applied TF analyses to beat-to-beat RR time-series data extracted from electrocardiograms of 30 healthy adults during three stress tasks: mental calculation, noise exposure, and cold pressor test. *Approach.* Continuous wavelet transform (CWT), and ensemble empirical mode decomposition (EEMD) were compared to the standard short-term Fourier transform (STFT). Signals were divided into anticipation, stress, and recovery periods. *Main results.* When analysed in 30 s windows, all three methods detected dynamic time variations in standard frequency bands (low-frequency (LF) [0.04–0.15 Hz], high-frequency (HF) [0.15–0.40 Hz]) during stress compared to baseline. Compared to SFFT, EEMD and CWT showed greater sensitivity than STFT to identify LF and HF differences. Spectrograms identified regions of interest outside standard frequency bands, where CWT provided superior temporal and frequency resolution, especially at low frequencies. While EEMD spectrograms were uninterpretable, analysis of individual EEMD modes enabled tracking instantaneous changes in both frequency and amplitude. *Significance.* In conclusion, CWT and EEMD proved most valuable for identifying patterns in stress-evoked HRV and providing information on autonomic nervous system activation latency, responsiveness, and adaptability.

1. Introduction

The stress response involves complex interactions between central and peripheral systems that are designed to help us adapt to external threats. The autonomic nervous system (ANS) controls this process by balancing the activation of its two branches, the parasympathetic (PNS) and sympathetic (SNS) nervous systems. This allows for rapid physiological responses while supporting essential functions such as digestion (Godoy *et al* 2018).

In the presence of an acute stressor, the SNS becomes active and the PNS, which is dominant at rest, becomes lessened (Berntson *et al* 2016). The SNS and the PNS each exert reciprocal effects on cardiac sinus node activity, maintaining tonic activity but responding on different timescales. In terms of onset dynamics, muscarinic receptor stimulation (PNS) is directly coupled to the opening of potassium

channels (IK, ACh) within approximately 100 ms, whereas β-adrenergic receptor stimulation (SNS) is coupled to the slower process of second messenger (cAMP) production via enzymatic action over several seconds. Additionally, the enzymatic degradation of acetylcholine is very fast (rapid offset dynamics). Therefore, the PNS, driven by respiration, acts and dissipates rapidly, typically in less than a second. In contrast, the effects of the SNS in response to stressful stimuli take over five seconds to develop (Irisawa *et al* 1971, Mokrane and Nadeau 1998, Hainsworth 2004). ANS actions, sometimes referred to as 'oscillators'(Echeverría *et al* 2001), exert chronotropic effects on the heart by modulating the intervals between heartbeats. A single interbeat interval (RR) can reflect the complex interactions between different systems (Reyes Del Paso *et al* 2013, Shaffer *et al* 2014). One non-invasive method of quantifying ANS activity is heart rate variability (HRV), which is based on analysing RR variations in the electrocardiogram. Time–frequency (TF) analysis enables transient oscillatory patterns to be identified, which are believed to reflect distinct regulatory mechanisms depending on the frequency band (Shaffer *et al* 2014).

The short-time Fourier transform (STFT) has previously been presented as a suitable method for extracting power spectra from short-duration signals, including those lasting several minutes, such as those used in laboratory stress tasks (Force 1996, Elsenbruch *et al* 2000, Shaffer and Ginsberg 2017). Power spectra obtained by STFT are usually averaged within predefined frequency bands. Examples include the high-frequency (HF) band (0.15–0.40 Hz), which is associated with respiratory sinus arrhythmia (Tonhajzerova *et al* 2016, Grossman 2024), and the low-frequency (LF) band (0.04–0.15 Hz) which is thought to reflect baroreflex mechanisms (Chapleau and Abboud 2004). However, one limitation of the STFT is that it assumes stationarity, at least for the duration of the analysed time window. Additionally, there is a TF precision trade-off: the accuracy of frequency information is limited by the time window compared to the signal's duration. Long windows have better frequency resolution than short ones but poor time resolution, while short windows provide better time resolution but poorer lower-frequency resolution. Therefore, the fixed window size used in STFT may not fully capture signals in the contexts of acute stress conditions where RR intervals are deeply modulated by multiple physiological mechanisms (McEwen 2007).

Two methods that could enhance the STFT for non-stationary signals are the continuous wavelet transform (CWT) and the ensemble empirical mode decomposition (EEMD), the latter being an extension of the EMD.

The CWT is commonly used to extract TF components from EEG time series data (Rhif *et al* 2019). The CWT defines a family of wavelets—mathematical functions that are localised in both time and frequency. Convolving these wavelets with a signal allows frequency components to be extracted over time, significantly improving the frequency resolution compared to the STFT, particularly for low frequencies. Therefore, the CWT has the potential to reveal lower oscillatory components that would otherwise be obscured by other methods. However, although the CWT can capture transient features from complex mechanisms (Samar *et al* 1999, Rhif *et al* 2019), it still assumes linearity (Farge 1992, Sadowsky 1996). This may not be the optimal approach for analysing nonlinear, non-stationary signals such as RR time series derived from ECGs.

EMD is a data-driven method with high TF resolution that avoids assumptions of stationarity and linearity completely (Wu and Huang 2009). Instead of testing a family of predefined frequencies of interest, EMD decomposes complex signals empirically into simple oscillatory components known as intrinsic mode functions (IMFs). The Hilbert–Huang transform (HHT) is then applied to these IMFs to convert them into instantaneous frequencies and amplitudes (Li *et al* 2011). EEMD is a noise-assisted data method that improves the performance of EMD by avoiding the mode mixing problem with minimal additional complexity (Mandic *et al* 2013). Thus, this EMD extension was used in our analysis. Compared to CWT, EEMD should improve accuracy at the instantaneous frequency (IF) level and thus be more sensitive to intrinsic, dynamic patterns.

The use of TF methods to extract HRV has been evaluated during resting conditions and during specific events such as dynamic movements, epilepsy, heart failure, sudden death, myocardial ischaemia, or anaesthesia (Gamero *et al* 1996, Echeverría *et al* 2001, Shafqat *et al* 2009, Li *et al* 2011, Omar and Mohamed 2011, Schiecke *et al* 2016, Cossul *et al* 2023). However, this topic is largely under-documented in the context of acute stress, with the work of Lee *et al* (2022) being an exception. Our study addresses this gap by comparing the performance of three HRV TF analysis methods during acute stress episodes: (1) STFT, (2) CWT, and (3) EEMD with HHT. In each acute stress episode, we studied dynamic changes in three phases: anticipation, in-task and recovery. We assessed the performance of the methods in capturing dynamic changes in three tasks in which the ANS (SNS and PNS) is thought to be differentially engaged: a) a mental (arithmetic) stress task, b) exposure to loud noise, c) the cold pressor test (CPT).

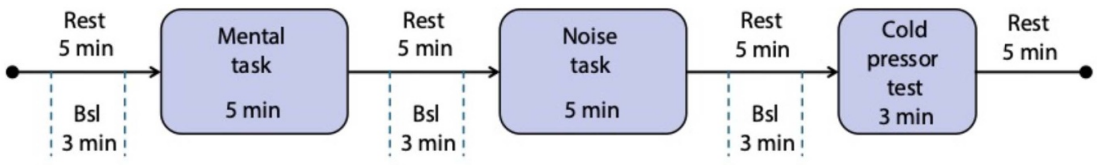

Figure 1. Stress induction procedure. Each task was of 5 min duration and presented in a predefined order. Abbreviations: bsl, baseline.

2. Methods

2.1. Participants and stress induction procedure

Thirty healthy young adults (15 females and 15 males aged 27.2 ± 3.9 years) underwent a multimodal stress induction protocol while seated in a soundproof booth (see figure 1). All participants had a normal body mass index (Mean = 22.8, SD = 3.0). Inclusion criteria required normal hearing thresholds (⩽15 dB HL at 0.5–4 kHz), normal loudness discomfort levels (⩾90 dB HL at 0.5–8 kHz), and good self-reported psychological and physical health. Exclusion criteria included diagnosed depression or anxiety disorders, use of medication affecting stress or cardiac function, hearing-related disorders, and any acute conditions affecting hearing on the day of testing (e.g. cold, sinusitis, Covid-19). Participants with Raynaud's disease, cerebral, respiratory, cardiovascular diseases, diabetes, hypoglycaemia, or pregnancy were also excluded. The study was approved by the University's Institutional Review Board, and all participants provided written informed consent.

The first task was a 5 min mental calculation derived from the Trier Social Stress Test (Kirschbaum *et al* 1993), in which participants were instructed to subtract 13 from a large number (e.g. 1022) under time pressure, until reaching the smallest positive number (e.g. 1022–13, 1009–13, etc). Errors or timeouts required a restarting from 1022. Participants performed the task autonomously and silently to control for breathing (Bernardi *et al* 2000, Thomas *et al* 2019). The second task was a 5 min exposure to LF broadband noise, delivered via frontal speakers. The noise increased exponentially from 40 to 90 dBA over the first 2 min, then remained at 90 dBA for the final 3 min. This level of noise has been shown to induce cortisol release (Waye *et al* 2002, Hebert and Lupien 2009). The final task was the CPT (Mitchell *et al* 2004, Mourot *et al* 2009), which is a painful task in which participants are asked to submerge their right hand in cold (6.5 °C) circulating water for 3 min. Rest periods of 5 min were added before and after each task to minimise carryover and allow for baseline and recovery. All participants were recruited via Facebook and poster advertisements at the Université de Montréal, and the study was approved by the university's internal review board, the Comité d'Éthique pour la Recherche Clinique.

2.1.1. Data collection

Raw ECG signals were acquired at 500 Hz using a Holter Recording system (Burdick, Model 6632, Cardiac Science, Deerfield, WI, USA) with a 5-lead configuration and were initially processed in Matlab using a custom R-peak detection algorithm (Dubé *et al* 1988). The extracted RR time series were validated using a combination of an in-house ECG analysis software VCGMI (Jacquemet *et al* 2011) and Burdick Vision Premier software (Cardiac Science, Bothell, WA, USA), with the latter managed by a trained physician. Ectopic beats, compensatory pauses, arrhythmic events, and segments of noisy signal were tagged and removed, and normal beats that may have been missed were manually added or interpolated from the local heart rate median. All analyses were performed using the validated time series consisting of normal sinus beats. They were resampled to 2 Hz using cubic spline interpolation and linearly detrended to remove slow drift.

2.2. Preprocessing

Once resampled and detrended, individual time series were padded with 20 s of reflected data. To avoid violating the assumptions of stationarity and linearity associated with Fourier analysis, we analysed the spectral components derived from three algorithms designed to improve the accuracy of the Fourier transform with respect to transient, nonlinear signals: STFT, CWT and EEMD. All analyses were performed with Python version 3.10 (Python Software Foundation 2021). STFT calculations were performed using the *SciPy* package, version 1.14.1 (Virtanen *et al* 2020). CWT calculations were performed using the *Clouddrift* package, version 0.44.0. The wavelet module of this package consists of a direct translation of the MATLAB implementation of the Morse wavelet by Lilly (2024). EEMD calculations

were performed using the *PyEMD* package, version 1.6.4 (Laszuk 2025). All three analyses removed frequencies above 0.4 Hz, which do not represent respiratory-linked ANS activity, and also removed frequencies below 0.0167 Hz, which is the limit imposed by our shortest analysis period (60 s).

2.3. STFT

The STFT is based on the assumption that a short portion of a non-stationary signal is stationary and thus can be analysed using the fast-Fourier transform (FFT; Elsenbruch *et al* 2000). Essentially, the calculation of the STFT involves applying the FFT within a defined window length and then sliding that window along the signal until the entire signal is processed.

The STFT of a signal $x(t)$ evaluated at time t and at frequency ω can be defined as

$$S_x(t, \omega) = \int_{-\infty}^{\infty} w(t - t')\, x(t')\, e^{-i\omega t'}\, dt'$$

where $w(t-t')$ represents the sliding convolution window.

The oscillatory power is computed by taking the log10 of the squared magnitude of S_x.

In our analysis, we used a 32 s Hann window, shifted by 5 s per iteration. The FFT length was 64 points, yielding 33 frequencies between 0 and 1 Hz. Frequencies below 0.0167 (none was present) or above 0.4 Hz were excluded, resulting in 12 final frequencies.

2.4. CWT

Wavelet decomposition involves breaking down a signal at different timescales using a 'mother wavelet ψ, modified by scaling parameter a, and positional parameter b:

$$\psi_{a,b}(t) = \frac{1}{\sqrt{a}}\psi\left(\frac{t-b}{a}\right);\ a > 0, -\infty < b < +\infty.$$

Given a signal $x(t)$, the CWT consists in a time (b)—scale (a) representation of the signal in terms of the following convolution,

$$W_x(a, b) = \int_{-\infty}^{\infty} x(t)\, \psi^*_{a,b}(t)\, dt$$

where $\psi^*_{a,b}$ is the scaled and shifted mother wavelet (Rhif *et al* 2019).

Similarly to the STFT, the wavelet applies a windowing function to the input signal. Here, the scale parameter varies as an inverse of the frequencies: the analysis window (the wavelet) used in the CWT effectively becomes a low frequency oscillation at large scale ($a > 1$), and a high frequency oscillation at short scale ($a < 1$), improving time resolution.

We chose the Morse wavelet as the mother wavelet because of its high flexibility and suitability for transient signals with rapidly changing frequency content (Lilly 2024). The Morse wavelet corresponds to a family of analytic wavelets defined by a generalised exponential function parameterised by β and γ, which control its TF localisation and symmetry properties. This parameterisation allows for a high degree of flexibility in adjusting the time and frequency resolution. For our analyses, β was set to 20 (high frequency resolution) and γ was set to 3 (high frequency decay); a configuration that emphasises frequency resolution over time resolution. We selected 100 logarithmically spaced frequency bins between 0.0167 and 0.4 Hz. Once transformed, the oscillatory power was computed by taking the $\log_{10}$ of the squared magnitude of the transformed signal.

2.5. EEMD

The EMD decomposes a signal into intrinsic oscillatory modes through an empirical 'sifting' process derived from the structure of the data. The process, described in detail in Huang *et al* (1998), involves creating upper and lower envelopes of the signal by interpolating local maxima and minima, and then subtracting the mean of these two envelopes from the original data. Repeated siftings make the data progressively less complex until it satisfies two conditions:

1. The number of extrema and zero-crossings are approximately equal.
2. The mean of the upper and lower envelopes is zero.

This results in an IMF, which consists of an oscillatory component that varies in amplitude and frequency with time, with no riding waves, and is symmetric around zero. Once the first IMF is

reached, the first residue is extracted by subtracting the IMF from the original signal, and this residue becomes the new data for further sifting to extract subsequent IMFs. Sifting continues until the standard deviation between siftings falls below a threshold, at which point the final residue is calculated from the last IMF. The original signal can be reconstructed from the sum of the IMFs and the final residue, demonstrating that the original signal has been decomposed into empirical modes plus the final residue. For interested readers, a step-by-step tutorial of the sifting procedure and the derivation of IMFs similar to the one used can be found in the EMD Python package (Quinn 2019).

The EEMD extends this process slightly by adding a small amount of Gaussian noise to the original signal before extracting the IMFs. We chose a noise width of 0.05 based on the recommendations of Wu and Huang (2009), who showed that a noise amplitude of 0.1–0.4 times the standard deviation of the signal provides optimal ensemble averaging while maintaining signal fidelity. The more conservative value of 0.05 was selected to minimise potential distortion of the RR intervals signal structure while still achieving the noise-assisted decomposition benefits of EEMD, particularly for mitigating mode-mixing effects. After noise addition, the full EMD process is repeated several times, and the resulting IMFs are averaged. This reduces the sensitivity of EMD to noise in the original signal and reduces mode mixing (Wu and Huang 2009), where a frequency component is spread across multiple modes. In our analysis, the calculation of the IMFs was repeated 100 times before averaging. This process resulted in at least 5 extracted IMFs for each input signal, regardless of basal, stress tasks, pressor test or recovery conditions in all 358 recordings. Any IMFs that could have been identified after the 5th IMF were not extracted and analysed. Specifically, for IMF1, a correlation was calculated between the original signal and the IMF. IMF1 showed consistently low correlation (<0.2) with the original RR interval signal, indicating it primarily represented HF measurement artefacts or non-physiological noise. This is documented in the supplementary materials, where IMF1 is clearly representing non-physiological aspects of the input signal, such as HF noise as well as the artefact created by the reflected data used to pad the signal. Also in the supplementary materials is a figure showing the frequency excursion of each IMF (from IMF2 to IMF4), as represented by the inter-quartile range for the IF for each condition and task period, averaged across participants.

IMF1 and IMF5 were excluded from analyses. IMF1 (frequency range: 0.2232–0.3413 Hz) was excluded because it predominantly captures HF oscillations that likely represent measurement noise and HF artefacts, the added noise from the EEMD procedure, and artefacts from data processing). For the vast majority of participants and conditions, IMF1 did not correlate with the original signal ($r < 0.2$), suggesting that it captured HF noise. The supplementary illustration of the EEMD method also shows this sensitivity of IMF1 to HF noise and processing artefacts. IMF5 (frequency range: 0.0182–0.0217 Hz) was excluded from analysis when present because this frequency range is below our specified analyses range (0.0167–0.4 Hz). These ultra-low frequencies are not typically associated with acute autonomic responses to stress.

The IF and amplitude of each IMF are then obtained by the HHT as follows: For each IMF, the Hilbert Transform was applied to obtain the analytic signal. The magnitude of the analytic signal provides the instantaneous amplitude, which is squared to calculate the power. The TF spectrum was constructed by computing IF for each IMF via the Hilbert transform, binning IF values into 100 logarithmically-spaced frequency bins (0.0167–0.4 Hz), and accumulating Power(t) from IMFs whose IF falls within that bin for each time point and frequency bin. Lastly, we added 1 to the power of the HHT before computing the log-power to maintain the value of 0 for TF bins with zero observations.

2.6. Statistical analysis

2.6.1. Spectra

Data were averaged within two frequency bands defined from the literature (LF: 0.04–0.15 Hz; HF: 0.15–0.40 Hz) (Force 1996, Shaffer and Ginsberg 2017). For each subject and task, the average log-power of the 3 min baseline period was calculated, and the difference from baseline was determined at each time point for both frequency bands. These two time-series were then averaged over 30 s windows, which were treated as categorical time points to evaluate changes in HF and LF powerband spectra over time. The 'stress response' period was extended to 60 s before and after the tasks to include anticipation and recovery. Statistical analyses were performed using R 4.3.1 (2023) on RStudio 2023.9.1 (Posit Software PBC, Boston, USA). Interactions and main effects of time and frequency bands on power changes were tested for each task using linear mixed effects models with the *lme4* R package (Bates *et al* 2014). Random effects were subject related, and models were controlled for sex. Pairwise comparisons were performed using the *emmeans* R package (Lenth 2024), which is based on least square means and corrected for multiple comparisons with Tukey adjustment. For the main effect of time (across frequency bands), each time point was compared to baseline. To examine the respective contributions of the two standard

Table 1. Mean HR values (in bpm) for each period. Values are averaged over the entire stress duration.

	Mental task Mean (SD)	*P* value	Noise task Mean (SD)	*P* value	CPT task Mean (SD)	*P* value
Baseline	71.3 (10.2)		70.1 (9.6)		70.5 (10.1)	
Stress period	79.2 (14.7)	<.0001	69.6 (10.0)	<.05	75.0 (11.9)	<.05

frequency bands (LF and HF) at each time point, the latter were also compared with one another. The alpha level for statistical significance was set at 0.05.

2.6.2. Spectrograms

The sampling period of the TF representation was 5 s for STFT and 500 ms for CWT and EEMD methods. Within each frequency, the average log-power of the 3 min baseline period was calculated for each subject and task, and the difference from baseline was determined at each time point. Spectrograms were plotted for all three methods.

Significant clusters were identified using a nonparametric one-sample t-test at the cluster-level with a permutation test for p-value correction, i.e. a method developed for EEG/MEG data (Maris and Oostenveld 2007), and implemented in the Python package *mne* version 1.8.0 (Gramfort *et al* 2013). Significant clusters are shown in full colour in the spectrograms, while non-significant clusters are shown semi-transparently for context.

For the CWT spectrograms, significant clusters were used to empirically define regions of interest (ROIs) in frequency and time, identified by black rectangles in figure 4. The unsubtracted log power in these ROIs was averaged for both task and baseline and plotted as bar graphs. A repeated measures t-test was performed to confirm the significant differences between task and baseline for each ROI.

3. Results

3.1. Effects of stress tasks on heart rate

The results indicate that, on average (over the entire duration of the tasks), all tasks had a significant effect on HR compared to their respective baseline. Mean HR increased significantly during both the Mental ($t(29) = 4.53$, $p < .0001$, with means bpm 71.3 ($\pm$10.2) and 79.2 ($\pm$14.7) for the baseline and task, respectively) and CPT tasks ($t(29) = 2.60$, $p < .05$, with means bpm 70.5 ($\pm$10.1) and 75.0 ($\pm$11.9) for the baseline and task, respectively), indicating that the mental and CPT tasks were effective in inducing stress. However, mean HR decreased significantly during the noise task ($t(29) = -2.38$, $p < .05$), with means bpm of 70.1 ($\pm$9.6) and 69.6 ($\pm$10.0) for baseline and task, suggesting that it may not have been as stressful as the two other tasks, or that noise involved a different type of response. Mean HR values are shown in table 1.

3.2. Comparison of baseline period TF spectra

Figure 2 shows the full spectra for baseline period preceding each task period, as processed by each of the three methods. To assess baseline comparability, we conducted statistical comparisons of LF and HF power across the three baseline periods for all TF methods. Friedman tests (non-parametric repeated measures) revealed no significant differences between baselines for any method or frequency band (all $ps > .05$).

3.3. Comparison of total and predefined low—and high—frequency band spectra

The time course of power changes, independent of frequency bands, varied between tasks (see figure 3). Significant main effects of time were observed during the Mental task for all three methods (STFT: $F(14, 841) = 8.63$, $p < .0001$; CWT: $F(14, 841) = 9.96$, $p < .0001$; and EEMD: $F(14, 841) = 8.11$, $p < .0001$), and during the noise task for all three methods (STFT: $F(14, 841) = 2.96$, $p = .002$; CWT: $F(14, 841) = 3.37$, $p < .0001$; and EEMD: $F(14, 841) = 2.97$, $p = .002$). During the CPT task, differences were observed for STFT ($F(10, 601) = 2.41$, $p < .009$) and CWT ($F(10, 601) = 2.69$, $p = .0032$), but not for EEMD $F(10, 601) = 1.05$, $p = .40$). In the Mental task, differences were evident at the onset while the noise task did not reveal any significant differences at specific time points. Overall, there were few differences between the methods regarding total power. Time windows with significant total power differences are indicated by black stars in figure 3.

When analysed separately, the standard LF (0.04–0.15 Hz) and HF (0.15–0.40 Hz) frequency bands exhibited diverging temporal variations in the noise and CPT tasks, but not in the Mental stress task (all $Fs < 1$ for the TF band interaction in all three methods) (figures 3(A)–(C)). In the noise task, all three

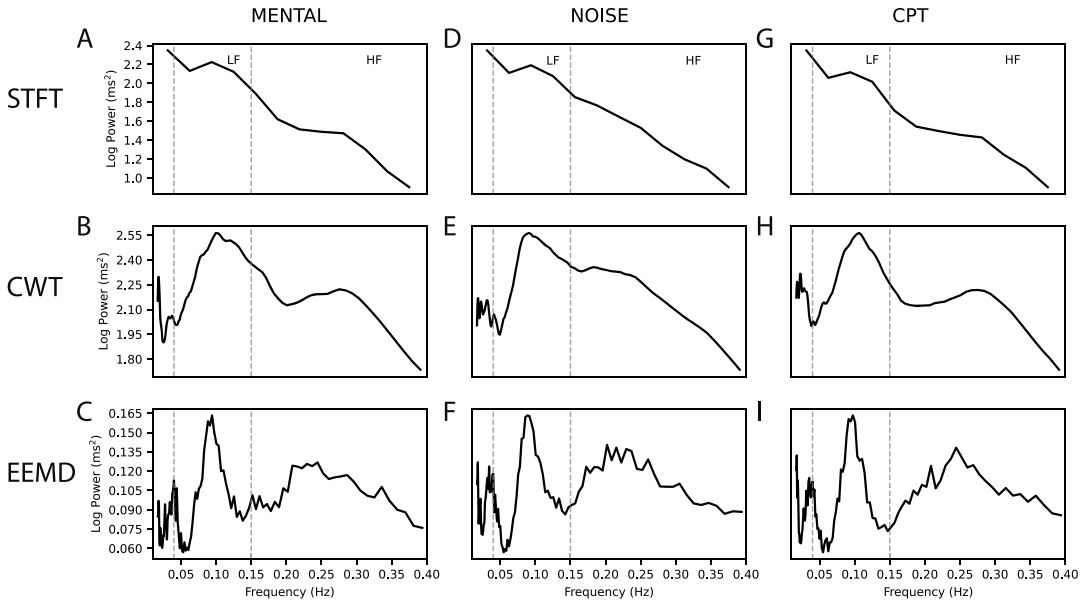

Figure 2. Log power spectrum (ms^2) of the baseline periods preceding each stress task (mental, noise, and cold pressor test) as processed by the short-time Fourier transform (STFT), Continuous Wavelet transform (CWT), and ensemble empirical mode decomposition (EEMD).

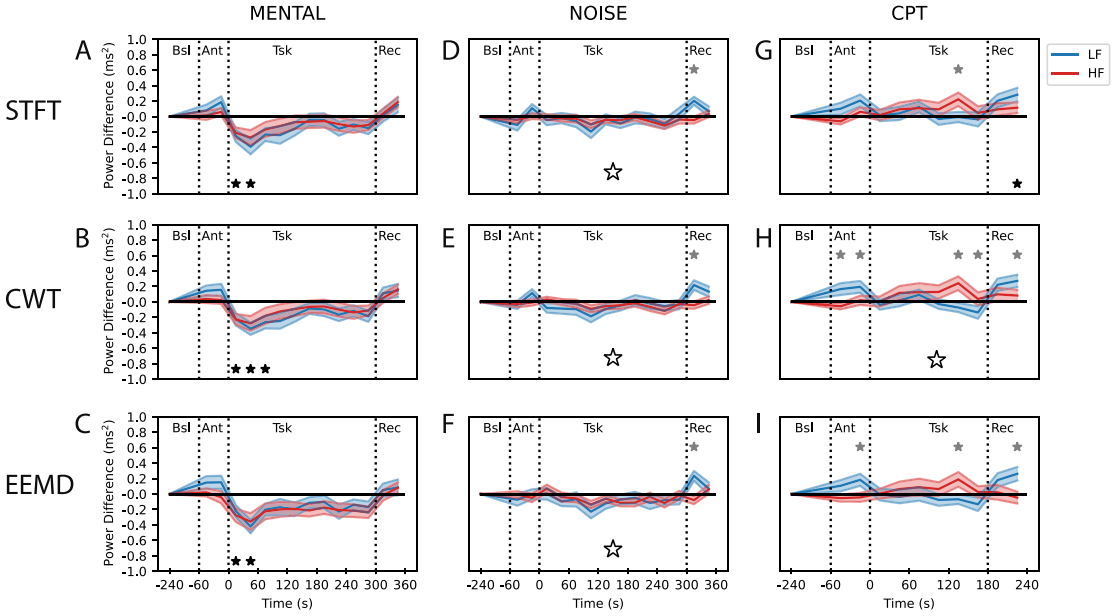

Figure 3. Comparison of the variation in the low-frequency (LF) and high-frequency (HF) band power spectra, as extracted by the three methods across three acute stress conditions: Mental arithmetic, noise exposure, and the cold pressor test. The red and blue lines illustrate the temporal variation in mean power change from baseline in the LF (0.04–0.15 Hz) and HF (0.15–0.4 Hz) bands, respectively. The shaded area around the curves represents the standard error of the mean (SEM). All methods show consistent variation in power over time. Small black stars indicate that total power, regardless of frequency band (LF + HF), differs from baseline. Large black stars indicate a main effect of time in cases where there were no significant pairwise comparisons. Small grey stars indicate interactions between time and frequency band. Values are log-transformed and expressed in terms of power difference from baseline in ms^2. Each time point is labelled with the start time of the 30 s time window. Abbreviations: Ant, anticipation; Bsl, baseline; EEMD, ensemble empirical mode decomposition; HF, high frequency band; LF, low frequency band; Rec, recovery; STFT, short-term Fourier transform; Tsk, task. Significant code: * $p < .05$.

methods captured an increase in the LF vs. HF frequency band at time 300, with all p-values less than .001. (figures 3(D)–(F)). In the CPT task (figures 3(G)–(I)), the interaction between time and frequency bands was significant for all three methods. However, the CWT was more sensitive than the other two methods at detecting differences between LF and HF at different time points (figure 3(I)). STFT was

the least sensitive, detecting only one difference between the LF and HF frequency bands (figure 3(H)). Overall, apart from a few minor differences, all methods identified broadly similar temporal patterns when considering predefined LF (0.04–0.15 Hz) and HF (0.15–0.40 Hz) frequency bands.

3.4. Visual comparison of spectrograms

Spectrograms of the log-transformed power were plotted for each stress type (figure 4). Dashed black boxes illustrate the significant clusters ($p < .05$), which were identified by the permutation cluster test. Nonsignificant regions are plotted semitransparently for context. Across tasks, the clusters identified by STFT appeared similar to those identified by CWT, but were more diffuse across frequencies. For instance, during the mental task, the STFT identified a significant cluster during recovery between 0 and 0.08 Hz (figure 4(B)), whereas the CWT identified it within a more precise frequency range of 0.025–0.06 Hz (figure 4(C)). Another example is the identification of an LF increase during the anticipation of stress followed by an HF decrease at the onset of the task, which was identified by the CWT in the Mental stress task. The STFT identified the HF decrease, but not the LF increase (figures 3(B) and (C)). Consistently, across tasks, CWT clusters were more concentrated within identifiable frequency boundaries. In contrast, STFT clusters were visually blurred at lower frequencies due to STFT's reduced frequency resolution at those frequencies. However, CWT identified clusters across wider time windows than STFT did (figures 4(E) and (F)), largely due to the chosen parameterisation of CWT, which emphasises frequency over time resolution. Conversely, the TF representation with EEMD produces very high time and frequency resolutions, revealing the true complexity of frequency changes over time in the RR interval series. Regarding EEMD, similar regions of increased and decreased power can be observed when compared to STFT or CWT; however, the high TF resolution of EEMD greatly complicates any visual interpretation of its spectrogram.

3.5. Empirically defined TF ROIs

A visual analysis of the spectrograms revealed that the observed changes in HRV power did not neatly fall into the standard LF (0.04–0.15 Hz) and HF (0.15–0.4 Hz) bands, especially when using the CWT method. Instead, significant clusters most often spanned two frequency bands. To determine the true statistical power of these effects, TF ROIs based on the clusters identified by a cluster-based permutation test were defined for the CWT results only (see figures 4(C), (F) and (I). Comparisons of the log power changes in these ROIs with baseline values in the same frequency bands revealed a significant increase from baseline between 0.025 and 0.035 Hz during the entire anticipation period ($t(29) = -3.41$, $p < .01$) and recovery period ($t(29) = -4.71$, $p < .0001$). A significant decrease was also observed between 0.05 and 0.3 Hz during the first 60 s of the mental task ($t(29) = 4.6$, $p < .001$). For the noise task, a significant increase was observed between 0.025 and 0.05 Hz throughout the recovery period ($t(29) = -6.02$, $p < .0001$). For the CPT task, a significant increase was observed between 0.028 and 0.05 Hz during the anticipation and recovery periods ($t(29) = -3.82$, $p < .001$ and ($t(29) = -4.03$, $p < .001$, respectively).

3.6. Independent IMF components

It was difficult to interpret the representation of the mean HHT power on the EEMD spectrograms across participants. As a secondary approach, we examined the differences in power and IF for each mode individually.

Figure 5 shows the time course of full-spectrum power variation for each mode individually, averaged across participants and tasks. The colour of each line represents the average IF measured at that time point across participants. As can be seen from the range of instantaneous frequencies, IMF2 represents the middle of the HF band, IMF3 represents the upper of the LF band, and IMF4 represents the lower LF band. All frequency values and ranges are shown in table 2. The frequency excursions for each IMF can be found in Supplementary. Significant main effects of time were observed during the mental and CPT tasks across all three modes (Mental: IMF2: $F(14, 406) = 9.44$, $p < .0001$; IMF3: $F(14, 406) = 3.02$, $p < .001$; IMF4: $F(14, 406) = 6.98$, $p < .0001$; CPT: IMF2: $F(10, 286) = 1.85$, $p = .05$; IMF3: $F(10, 286) = 4.00$, $p < .0001$; IMF4: $F(10, 286) = 4.17$, $p < .0001$). Significant main effects of time were also observed during the noise task for IMF2 ($F(14, 402) = 2.02$, $p < .05$) and IMF4 ($F(14, 402) = 7.25$, $p < .0001$).

Pairwise comparisons revealed a significant decrease in IMF 2 power during the mental task during the first 150 s. The mean IMF during this period was 0.22 Hz (SD: 0.026; range: 0.16–0.27). Another significant decrease in power occurred between 210 and 270 s, with a mean IMF of 0.21 Hz (SD: 0.030; range: 0.17–0.26). Significant increases in power were also found for mode 4 during the mental task between 300 and 360 s (mean IF: 0.03 Hz; SD: 0.005; range: 0.02–0.04), during the noise task between

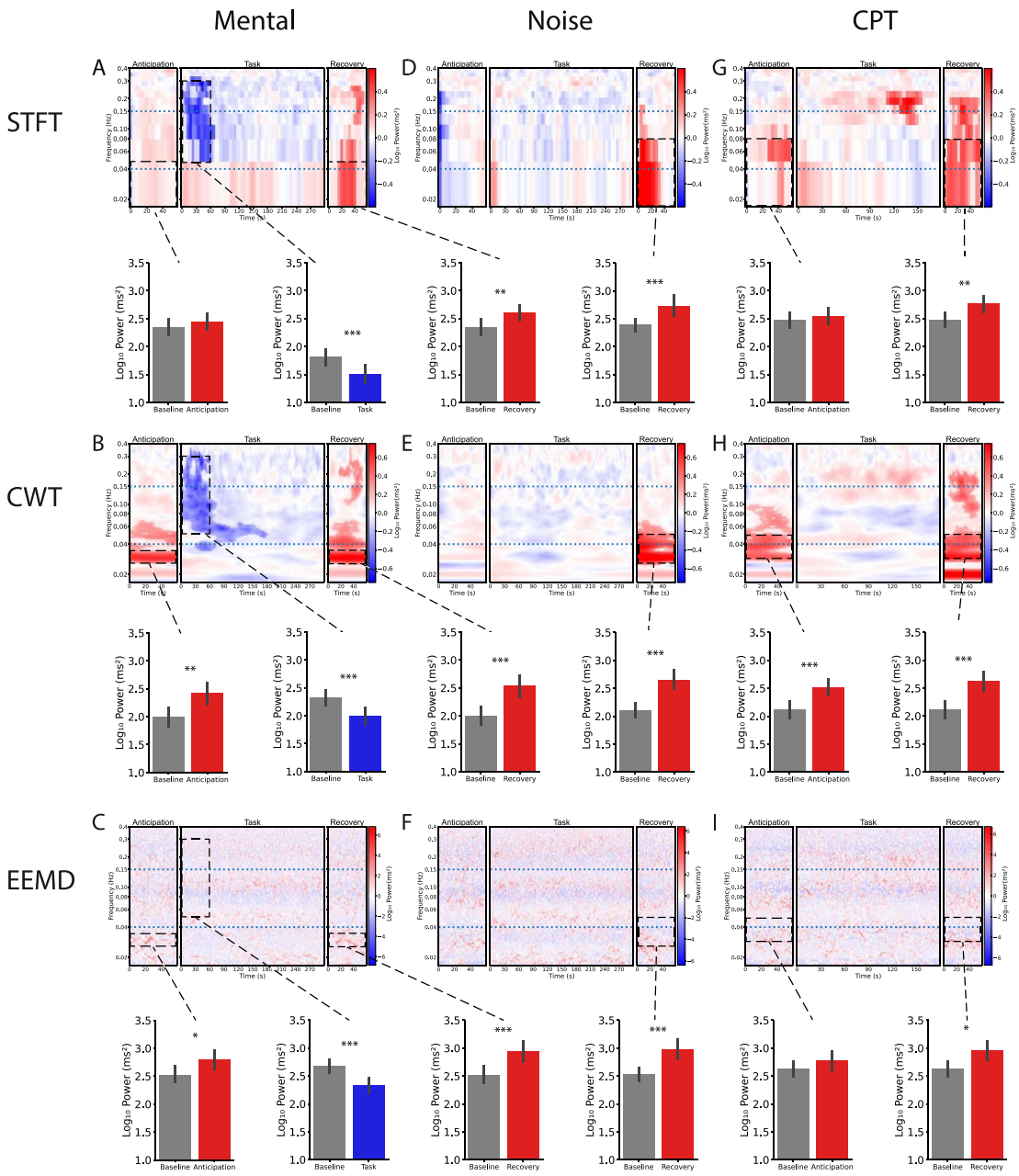

Figure 4. Time–frequency plots of the log-power difference from the baseline of RR intervals for each method: STFT, EEMD, and CWT, for each task. The anticipation and recovery periods are also shown. The change in power is represented by the colour scale, where red indicates an increase from baseline and blue indicates a decrease. Regions with darker colours indicate significant changes from baseline, as identified by cluster-level one-sample *t*-tests. Dashed boxes indicate regions of interest (ROIs), which delineate the time and frequency ranges of regions of significant change. ROIs are identified using cluster-based permutation tests (for CWT only). Bar graphs show the difference between ROIs and baseline log-power in the same frequency bands. Abbreviations: CPT, cold pressor test; EEMD, ensemble empirical mode decomposition; STFT, short-time Fourier transform. Signification codes: * $p < .05$, ** $p < .01$, *** $p < .001$.

300 and 330 s (mean IF: 0.03 Hz; SD: 0.006; range: 0.02–0.04), and during the CPT task between 180 and 210 s (mean IF: 0.03 Hz; SD: 0.006; range: 0.02–0.05).

4. Discussion

This study compared three methods for extracting frequency power variation from RR intervals: the STFT, the CWT, and the EEMD. Our results clearly show that, overall, TF analysis is generally suitable for describing the time course and complexity of HRV signals under laboratory stress conditions. To our knowledge, this is the first study to evaluate the TF resolution of various methods for extracting HRV during acute stress.

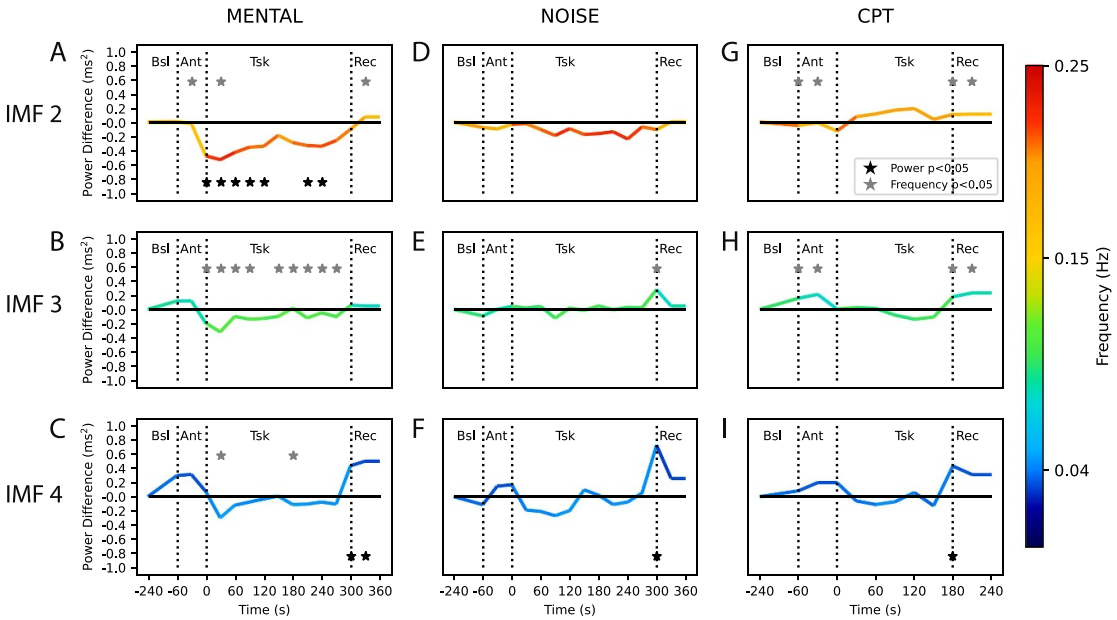

Figure 5. Time course of power and frequency variation within each independent component of the RR interval spectrum (IMF) extracted using EEMD. In the mental task, a decrease in IMF2 power is observed during the task (panel (A)) which is also associated with an increase in IMF3 frequency (panel (B)). Across all tasks, the recovery period was associated with an increase in IMF4 power (panels (C), (F), (I)). This power increase was associated with a decrease in IMF2 and IMF3 frequency, particularly for the CPT task (panels (G), (H)). The increase in low frequencies (IMF 4, panel F) during recovery suggests that changes in RR originate from different physiological sources with variable activation times. For each line, the *y*-axis position represents the power difference from baseline, and the colour represents the mean instantaneous frequency. The full colour scale shows the frequency range across the IMFs.

Table 2. Mean, standard deviation (SD) and range of the frequencies identified in each IMFs extracted with EEMD for each task.

	Mental task Mean (SD) [range]	Noise task Mean (SD) [range]	CPT task Mean (SD) [range]
IMF2	0.2 (0.018) [0.17–0.23]	0.21 (0.017) [0.18–0.23]	0.19 (0.014) [0.17–0.21]
IMF3	0.1 (0.011) [0.08–0.11]	0.09 (0.007) [0.08–0.1]	0.09 (0.008) [0.08–0.1]
IMF4	0.04 (0.005) [0.03–0.05]	0.04 (0.005) [0.03–0.05]	0.04 (0.003) [0.03–0.04]

Our main findings can be summarised as follows: First, HRV signals are dynamic and not stationary over time during stressful events. All three methods detected time variations from baseline. The mental stress task caused a significant decrease in power at its onset. The noise task produced general, unspecified dynamic time effects. The CPT task also showed time variations, but these were almost entirely dependent on the standard LF and HF frequency bands.

Second, spectrogram visualisations of HRV data using CWT or STFT transforms provide additional frequency resolution. These visualisations suggest that the standard LF-HF frequency bands may be inappropriate under stressful conditions. However, when using EEMD, which has very high TF resolution, the spectrogram becomes uninterpretable.

Third, EEMD demonstrates greater sensitivity in detecting transient changes in power, especially when modes are examined individually. Tracking changes in instantaneous power and frequency across EEMD components (IMFs) can reveal information about different physiological mechanisms.

Finally, frequencies that characterise transient changes in power can best be empirically defined using either CWT, which identifies ROIs, or EEMD, which measures the IF of the mode.

4.1. Sensitivity in standard LF-HF bands

The time course of power variation in the standard LF and HF frequency bands revealed that HRV is not stationary during a stressful event. Dynamic changes were observed fairly consistently across all methods. All three methods identified differences in the standard LF and HF bands during the noise and CPT tasks. However, the STFT was the least sensitive to these contrasts. This probably reflects the STFT's lower temporal resolution at lower frequencies compared to the other two methods. This is an inherent limitation of the STFT. The CWT was clearly the most sensitive method.

4.2. Spectrograms for visualising HRV data

Spectrograms are an easy way to visualise power variation over time and frequency. However, compared to STFT, CWT showed greater resolution at lower frequencies, making it easier to isolate task-specific effects in specific frequency bands. Wavelet results showed consistent frequency resolution at both high and low frequencies, enabling easy identification of ROIs. EEMD spectrograms demonstrated superior accuracy and sensitivity to transient events, with resolution independent of frequency. However, the spectrograms were visually uninterpretable, which prevented the identification of significant ROIs.

4.3. Empirically decomposed frequency bands

We used a cluster-level, one-sample *t*-test on the spectrogram data allowed us to identify new ROIs, specifically task-specific effects with empirically defined frequency ranges. The frequency power within these ROIs likely originates from different mechanisms, which suggests inter-individual variability in the oscillation frequency of physiological components. The empirically defined ROIs clearly demonstrate that the effects observed in our data often overlap two or more of the standard frequency bands, questioning the relevance of defining arbitrary frequency ranges *a priori* (Echeverría *et al* 2001).

4.4. Relevance of EEMD in HRV signals

Nonlinear indices in the time domain, such as sample entropy, approximate entropy, Poincare plots, and correlation dimension, account for irregularities in cardiac dynamics. These indices have often been considered suitable for describing RR intervals (Richman and Moorman 2000, Melillo *et al* 2011, Francesco *et al* 2012, Bolea *et al* 2014, Milena *et al* 2023). However, unlike TF analysis, they do not provide frequency information about the signal. Both CWT and STFT provide frequency information, but only EEMD is a non-linear, adaptive analysis method well-suited for highly transient stress events (Cheema and Singh 2019, Feradov *et al* 2022, Lee *et al* 2022). Our results show that, during a stress event, the oscillatory information carried by each IMF—particularly IMF2 and IMF4—varies in amplitude and frequency and is not completely stable over time (figure 5). This is contrary to the assumptions of linear transforms (Montano *et al* 2009).

When we analysed the oscillatory power within individual EEMD modes separately, we observed a dissociation of effects. The lower frequency effects associated with recovery from stress were contained in IMF 4, while the higher-frequency effects associated with the task itself were contained in IMF 2. IMF 3 did not show statistically significant differences in the time course of any of the three tasks. Furthermore, analysing the instantaneous frequencies within each mode provided a more precise empirically defined frequency range for each effect than CWT did. For IMF 2, we also observed that as the power of the frequencies observed decreased, the IF of IMF 3 increased. In general, power decreases were associated with frequency increases, and vice versa. These results suggest that, for EEMD, it may be more useful to observe how both power and frequency vary over time, as opposed to the standard method of observing how power varies over both frequency and time.

4.5. Physiological inferences about dynamic changes in IMFs

On the one hand, our results indicated differential activation depending on the stress phase. At the beginning of the mental task, power decreased at higher frequencies (around 0.30 Hz) while during recovery power increased at frequencies below 0.10 Hz. These findings suggest withdrawal of higher frequencies reflects the allocation of cognitive resources to the task while low frequencies reflect stress recovery mechanisms, and to some extent (although nonsignificant here), stress preparation.

On the other hand, we observed slight variation in the frequencies composing each EEMD mode over time. Previous research has speculated that each IMFs may index real physiological processes (Echeverría *et al* 2001). Although the underlying mechanisms responsible for these oscillatory changes are unclear, they confirm that the ANS acts as a complex dynamical system involving multiple physiological processes (Echeverría *et al* 2001, Berntson *et al* 2016, Brooks *et al* 2021).

4.6. Critics and limitations of our stress protocol

One limitation of this study was the absence of a subjective measure of perceived stress. As shown in table 1, mean HR changes between task and baseline differed significantly based on stress type. The mental task and CPT stressors significantly increased HR during the task, whereas the noise stressor slightly decreased HR. This suggests that the response patterns evoked by the tasks may not directly rely on the 'stress' level but rather on the levels of cognitive and emotional engagement, e.g. respectively low for the noise task, and high for the pain task (Bosch *et al* 2003, Seery 2013, Berntson *et al* 2016). Additionally, LF activations were observed during task anticipation and recovery for all three

tasks. These activations provided a basis for comparison that did not appear to be affected by the level of stress induced.

4.7. Clinical implications

Autonomic dysfunction, which is observed in chronic or stress-related conditions such as cardiovascular disease, diabetes, depression, post-traumatic stress disorder, neuropathic pain, and tinnitus, may affect stress reactivity and cardiac dynamics (Datzov *et al* 1999, Fadul *et al* 2010, Thayer *et al* 2010, Evans *et al* 2013, Brudey *et al* 2015, Huang *et al* 2017, Yeater *et al* 2021, Yu and Lee 2021, Rawn and Keller 2022, Manohar *et al* 2023). Due to their ability to track changes in HRV power and frequency, TF analysis, particularly CWT and EEMD, are valuable tools for identifying patterns in the stress-evoked HRV time course that provide information on ANS activation latency, responsiveness, and adaptability.

5. Conclusions (recommendations)

Comparison of the STFT, CWT, and EEMD methods have shown that modern methods of analysing nonstationary and nonlinear signals can accurately describe the effects of acute stressors on HRV in both time and frequency domains. Changes in HRV are often quantified using a single value derived from an ECG recording of either 5 min (short-term HRV) or less than 3 min (ultra-short term HRV) (Shaffer and Ginsberg 2017). Our results show that, in response to a mental stressor, HRV in the LF and HF bands varied dynamically within the 5 min stress period. This variation was successfully identified by all three methods. However, EEMD appeared to be more sensitive to this effect than CWT, and CWT appeared to be more sensitive than STFT, suggesting that increasingly nonlinear methods better capture the HF effect. Interestingly, CWT performed slightly better than EEMD in detecting LF effects in the anticipation and recovery periods of the CPT task. This suggests that CWT is not strictly inferior to EEMD.

STFT and CWT provide spectrogram representations that, when combined with cluster-level statistical methods, allow the identification of statistical regions in time and frequency that characterise the observed effects. CWT spectrograms showed increased separation of the observed effects in frequency. The anticipation/recovery-related power increase occurred in a lower frequency range than the task-related power decrease. These ROIs were often observed in more than one standard frequency range, suggesting that using predefined frequency ranges may be misleading. Additionally, the CWT method can be adjusted for greater temporal or frequency resolution, offering more flexibility than the other two methods. Finally, although the EEMD method does not lend itself well to a spectrogram representation, an alternative approach can be taken. Instantaneous power and IF can be analysed separately, allowing for the precise identification of the frequency or frequency shift associated with a given power change. This strategy narrowed for the frequency range of the task-related power increases and decreases considerably.

Although TF analysis has been used to measure HRV under non-stationary conditions, it has not been used specifically under acute stress conditions (Huang *et al* 1998, Omar and Mohamed 2011, Mandic *et al* 2013). Our study is the first to demonstrate that time–frequency methods, such as CWT and EEMD, are best suited to describing HRV under stress conditions.

Acknowledgments

We thank Omar Mahiddine for carefully validating the raw electrocardiogram (ECG) signals. We also thank Frederik Desaulniers and Tomy Aumont for helping us develop the silent arithmetic task and set up the stress protocol. The study was approved by the Comité de la recherche at Université de Montréal (CERC, # CERC-20-017-D) and was conducted with the written and informed consent of all participants. The research was conducted in accordance with the principles embodied in the Declaration of Helsinki and in accordance with local statutory requirements.

This work was made possible thanks to a CIRCA studentship for B.V, an AUDACE-FRQ Grant for S H and A V, and a Natural Science and Engineering Research Council (NSERC) of Canada Grant for S H. The authors report no conflicts of interest.

Data availability statement

The data that support the findings of this study are openly available at the following URL/DOI:. URL/DOI: https://doi.org/10.5683/SP3/OOOYMB (Hébert 2025).

Supplementary Figure 1: available at http://doi.org/10.1088/1361-6579/ae3ec7/data1.
Supplementary Figure 2: available at http://doi.org/10.1088/1361-6579/ae3ec7/data2.
Supplementary Figure 3: available at http://doi.org/10.1088/1361-6579/ae3ec7/data3.
Supplementary Video 1: available at http://doi.org/10.1088/1361-6579/ae3ec7/data4.
Supplementary Video 2: available at http://doi.org/10.1088/1361-6579/ae3ec7/data5.

ORCID iDs

Bérangère Villatte 0000-0002-5800-4472
Sayeed A D Kizuk 0009-0004-0088-8254
Jean-Marc Lina 0000-0003-3600-601X
Alain Vinet 0000-0003-2474-5827
Sylvie Hébert 0000-0003-0214-3884

References

Bates D, Maechler M, Bolker B and Walker S 2014. lme4: linear mixed-effects models using eigen and S4 R package version 1.1-7
Bernardi L, Wdowczyk-Szulc J, Valenti C, Castoldi S, Passino C, Spadacini G and Sleight P 2000 Effects of controlled breathing, mental activity and mental stress with or without verbalization on heart rate variability *J. Am. Coll. Cardiol.* **35** 1462–9
Berntson G G, Cacioppo J T and Bosch J A 2016 From homeostasis to allodynamic regulation *Handbook of Psychophysiology* 4 edn, ed J T Cacioppo, L G Tassinary and G G Berntson (Cambridge University Press) pp 401–26
Bolea J, Pueyo E, Laguna P and Bailón R 2014 Non-linear HRV indices under autonomic nervous system blockade *2014 36th Annual Int. Conf. IEEE Engineering in Medicine and Biology Society* pp 3252–5
Bosch J A, de Geus E J, Veerman E C, Hoogstraten J and Nieuw Amerongen A V 2003 Innate secretory immunity in response to laboratory stressors that evoke distinct patterns of cardiac autonomic activity *Psychosom. Med.* **65** 245–58
Brooks J, Crone J C and Spangler D P 2021 A physiological and dynamical systems model of stress *Int. J. Psychophysiol.* **166** 83–91
Brudey C, Park J, Wiaderkiewicz J, Kobayashi I, Mellman T A and Marvar P J 2015 Autonomic and inflammatory consequences of posttraumatic stress disorder and the link to cardiovascular disease *Am. J. Physiol. Regul. Integr. Comp. Physiol.* **309** R315–21
Chapleau M W and Abboud F M 2004 The baroreceptor reflex: novel methods and mechanisms *Neural Mechanisms of Cardiovascular Regulation N J* Dun, B H Machado and P M Pilowsky ed (Springer) pp 1–29
Cheema A and Singh M 2019 Psychological stress detection using phonocardiography signal: an empirical mode decomposition approach *Biomed. Signal Process. Control* **49** 493–505
Cossul S, Andreis F R, Favretto M A and Marques J L 2023 The use of empirical mode decomposition on heart rate variability signals to assess autonomic neuropathy progression in type 2 diabetes *Appl. Sci.* **13** 7824
Datzov E, Danev S, Haralanov H, Naidenova V, Sachanska T and Savov A 1999 Tinnitus, heart rate variability, and some biochemical indicators *Int. Tinnitus J.* **5** 20–23
Dubé B, LeBlanc A, Dutoy J L, Derome D and Cardinal R 1988 PC-based ST-segment monitoring with the VCG *Engineering in Medicine and Biology Conf.* pp 1768–70
Echeverría J C, Crowe J A, Woolfson M S and Hayes-Gill B R 2001 Application of empirical mode decomposition to heart rate variability analysis *Med. Biol. Eng. Comput.* **39** 471–9
Elsenbruch S, Wang Z, Orr W C and Chen J D 2000 Time-frequency analysis of heart rate variability using short-time fourier analysis *Physiol. Meas.* **21** 229–40
Evans S, Seidman L C, Tsao J C, Lung K C, Zeltzer L K and Naliboff B D 2013 Heart rate variability as a biomarker for autonomic nervous system response differences between children with chronic pain and healthy control children *J. Pain Res.* **6** 449–57
Fadul N, Strasser F, Palmer J L, Yusuf S W, Guo Y, Li Z, Allo J and Bruera E 2010 The association between autonomic dysfunction and survival in male patients with advanced cancer: a preliminary report *J. Pain Sympt. Manage.* **39** 283–90
Farge M 1992 Wavelet transforms and their applications to turbulence *Annu. Rev. Fluid Mech.* **24** 395–457
Feradov F, Ganchev T, Markova V and Kalcheva N 2022 EMD-based features for cognitive load and stress assessment from PPG signals *2021 Int. Conf. on Biomedical Innovations and Applications (BIA)* vol 1 pp 62–65
Force T 1996 Heart rate variability: standards of measurement, physiological interpretation and clinical use. Task Force of the European Society of Cardiology and the North American Society of Pacing and Electrophysiology *Circulation* **93** 1043–65
Francesco B, Maria Grazia B, Emanuele G, Valentina F, Sara C, Chiara F, Riccardo M and Francesco F 2012 Linear and nonlinear heart rate variability indexes in clinical practice *Comput. Math. Methods Med.* **2012** 219080
Gamero L G, Risk M, Sobh J F, Ramirez A J and Saul J P 1996 Heart rate variability analysis using wavelet transform *Comput. Cardiol.* **1996** 177–80
Godoy L D, Rossignoli M T, Delfino-Pereira P, Garcia-Cairasco N and de Lima Umeoka E H 2018 A comprehensive overview on stress neurobiology: basic concepts and clinical implications *Front. Behav. Neurosci.* **12** 127
Gramfort A *et al* 2013 MEG and EEG data analysis with MNE-Python *Front. Neurosci.* **7** 267
Grossman P 2024 Respiratory sinus arrhythmia (RSA), vagal tone and biobehavioral integration: beyond parasympathetic function *Biol. Psychol.* **186** 108739
Hainsworth R 2004 Physiological background of heart rate variability *Dynamic Electrocardiography* ed M Malik and A J Camm pp 1–12
Hébert S 2025 Methods paper: time-frequency analysis V1 ed Borealis (https://doi.org/10.5683/SP3/OOOYMB)
Hebert S and Lupien S J 2009 Salivary cortisol levels, subjective stress, and tinnitus intensity in tinnitus sufferers during noise exposure in the laboratory *Int. J. Hyg. Environ. Health* **212** 37–44
Huang N, Shen Z, Long S, Wu M L C, Shih H, Zheng Q, Yen N-C, Tung C-C and Liu H 1998 The empirical mode decomposition and the Hilbert spectrum for nonlinear and non-stationary time series analysis *Proc. R. Soc. A* **454** 903–95
Huang W A, Boyle N G and Vaseghi M 2017 Cardiac innervation and the autonomic nervous system in sudden cardiac death *Card Electrophysiol Clin.* **9** 665–79
Irisawa H, Caldwell W M and Wilson M F 1971 Neural regulation of atrioventricular conduction *Jpn. J. Physiol.* **21** 15–25

Jacquemet V, Cassani González R, Sturmer M, Dubé B, Sharestan J, Vinet A, LeBlanc A R, Becker G, Kus T and Nadeau R 2011 Evaluation of a subject-specific transfer-function-based nonlinear QT interval rate-correction method *Physiol. Meas.* **32** 619–35
Kirschbaum C, Pirke K M and Hellhammer D H 1993 The 'Trier Social Stress Test'–a tool for investigating psychobiological stress responses in a laboratory setting *Neuropsychobiology* **28** 76–81
Laszuk D 2025 PyEMD: Python implementation of empirical mode decomposition (EMD) and EEMD (Version 1.6.4) GitHub (available at: https://github.com/laszukdawid/PyEMD)
Lee S, Hwang H B, Park S, Kim S, Ha J H, Jang Y, Hwang S, Park H K, Lee J and Kim I Y 2022 Mental stress assessment using ultra short term HRV analysis based on non-linear method *Biosensors* **12** 465
Lenth R 2024 emmeans: estimated marginal means, aka least-squares means R package version 1.10.6
Li H, Kwong S, Yang L, Huang D and Xiao D 2011 Hilbert-Huang transform for analysis of heart rate variability in cardiac health *IEEE/ACM Trans. Comput. Biol. Bioinform.* **8** 1557–67
Lilly J M 2024 jLab: A data analysis package for Matlab v1.7.3 *Zenodo* (https://doi.org/10.5281/zenodo.4547006)
Mandic D P, Rehman N U, Wu Z and Huang N E 2013 Empirical mode decomposition-based time-frequency analysis of multivariate signals: the power of adaptive data analysis *IEEE Signal Process. Mag.* **30** 74–86
Manohar S, Chen G D, Li L, Liu X and Salvi R 2023 Chronic stress induced loudness hyperacusis, sound avoidance and auditory cortex hyperactivity *Hear Res.* **431** 108726
Maris E and Oostenveld R 2007 Nonparametric statistical testing of EEG- and MEG-data *J. Neurosci. Methods* **164** 177–90
McEwen B S 2007 Physiology and neurobiology of stress and adaptation: central role of the brain *Physiol. Rev.* **87** 873–904
Melillo P, Bracale M and Pecchia L 2011 Nonlinear heart rate variability features for real-life stress detection. Case study: students under stress due to university examination *Biomed. Eng.* **10** 96
Milena Č, Romano C, De Tommasi F, Carassiti M, Formica D, Schena E and Massaroni C 2023 Linear and non-linear heart rate variability indexes from heart-induced mechanical signals recorded with a skin-interfaced IMU *Sensors* **23** 1615
Mitchell L A, MacDonald R A and Brodie E E 2004 Temperature and the cold pressor test *J. Pain* **5** 233–7
Mokrane A and Nadeau R 1998 Dynamics of heart rate response to sympathetic nerve stimulation *Am. J. Physiol.* **275** H995–1001
Montano N, Porta A, Cogliati C, Costantino G, Tobaldini E, Casali K R and Iellamo F 2009 Heart rate variability explored in the frequency domain: a tool to investigate the link between heart and behavior *Neurosci. Biobehav. Rev.* **33** 71–80
Mourot L, Bouhaddi M and Regnard J 2009 Effects of the cold pressor test on cardiac autonomic control in normal subjects *Physiol. Res.* **58** 83–91
Omar M O A and Mohamed A S A 2011 Application of the empirical mode decomposition to ECG and HRV signals for congestive heart failure classification *2011 1st Middle East Conf. on Biomedical Engineering* pp 392–5
Python Software Foundation 2021 Python language reference version 3.10
Quinn A 2019 *Sifting* (version stable)—EMD tutorials *EMD documentation* Read the Docs(available at: https://emd.readthedocs.io/en/stable/emd_tutorials/01_sifting/index.html)
Rawn K P and Keller P S 2022 Habitual use of psychological coping strategies is associated with physiological stress responding during negative memory recollection in humans *Stress* **25** 30–39
Reyes Del Paso G A, Langewitz W, Mulder L J M, van Roon A and Duschek S 2013 The utility of low frequency heart rate variability as an index of sympathetic cardiac tone: a review with emphasis on a reanalysis of previous studies *Psychophysiology* **50** 477–87
Rhif M, Ben Abbes A, Farah I R, Martínez B and Sang Y 2019 Wavelet transform application for/in non-stationary time-series analysis: a review *Appl. Sci.* **9** 1345
Richman J S and Moorman J R 2000 Physiological time-series analysis using approximate entropy and sample entropy *Am. J. Physiol. Heart Circ. Physiol.* **278** H2039–49
Sadowsky J 1996 Investigation of signal characteristics using the continuous wavelet transform *J. Hopkins Apl. Tech. D* **17** 258–69
Samar V J, Bopardikar A, Rao R and Swartz K 1999 Wavelet analysis of neuroelectric waveforms: a conceptual tutorial *Brain lLang.* **66** 7–60
Schiecke K, Pester B, Piper D, Benninger F, Feucht M, Leistritz L and Witte H 2016 Nonlinear directed interactions between HRV and EEG activity in children with TLE *IEEE Trans. Biomed. Eng.* **63** 2497–504
Seery M D 2013 The biopsychosocial model of challenge and threat: using the heart to measure the mind *Soc. Personal. Psychol. Compass* **7** 637–53
Shaffer F and Ginsberg J P 2017 An overview of heart rate variability metrics and norms *Front. Public Health* **5** 258
Shaffer F, McCraty R and Zerr C L 2014 A healthy heart is not a metronome: an integrative review of the heart's anatomy and heart rate variability *Front. Psychol.* **5** 1040
Shafqat K, Pal S K, Kumari S and Kyriacou P A 2009 Empirical mode decomposition (EMD) analysis of HRV data from locally anesthetised patients *Annual Int. Conf. IEEE Engineering in Medicine and Biology Society 2009* pp 2244–7
Thayer J F, Yamamoto S S and Brosschot J F 2010 The relationship of autonomic imbalance, heart rate variability and cardiovascular disease risk factors *Int. J. Cardiol.* **141** 122–31
Thomas B L, Claassen N, Becker P and Viljoen M 2019 Validity of commonly used heart rate variability markers of autonomic nervous system function *Neuropsychobiology* **78** 14–26
Tonhajzerova I, Mestanik M, Mestanikova A and Jurko A 2016 Respiratory sinus arrhythmia as a non-invasive index of 'brain-heart' interaction in stress *Indian J. Med. Res.* **144** 815–22
Virtanen P *et al* 2020 SciPy 1.0: fundamental algorithms for scientific computing in Python *Nat. Methods* **17** 261–72
Waye K P, Bengtsson J, Rylander R, Hucklebridge F, Evans P and Clow A 2002 Low frequency noise enhances cortisol among noise sensitive subjects during work performance *Life Sci.* **70** 745–58
Wu Z H and Huang N E 2009 Ensemble empirical mode decomposition: a noise-assisted data analysis method *Adv. Data Sci. Adapt.* **1** 1–41
Yeater T D, Clark D J, Hoyos L, Valdes-Hernandez P A, Peraza J A, Allen K D and Cruz-Almeida Y 2021 Chronic pain is associated with reduced sympathetic nervous system reactivity during simple and complex walking tasks: potential cerebral mechanisms *Chronic Stress* **5** 24705470211030273
Yu T Y and Lee M K 2021 Autonomic dysfunction, diabetes and metabolic syndrome *J. Diabetes Investig.* **12** 2108–11